Surface Review and Letters, Vol. 21, No. 4 (2014) 1450059 (10 pages)

DOI: 10.1142/S0218625X14500590

SOLUTION PROCESSING OF CADMIUM SULFIDE BUFFER LAYER AND ALUMINUM-DOPED ZINC OXIDE WINDOW LAYER FOR THIN FILMS SOLAR CELLS

MAHBOOB ALAM[*,¶], MOHAMMAD ISLAM[*,†,‖], AMINE ACHOUR[‡], ANSAR HAYAT[*], BILAL AHSAN[*], HAROON RASHEED[*], SHAHZAD SALAM[§] and MOHAMMAD MUJAHID[*]

[*]*School of Chemical and Materials Engineering, National University of Sciences and Technology, Islamabad 44000, Pakistan*

[†]*College of Engineering, King Saud University, P. O. Box 800, Riyadh 11421, Saudi Arabia*

[‡]*Intégration de Systèmes de Gestion de l'Energie (ISGE), LAAS (CNRS), Toulouse, France*

[§]*State Key Laboratory of New Ceramics and Fine Processing, Department of Materials Science and Engineering, Tsinghua University, P. R. China*

[¶]*malam1999@hotmail.com*

[‖]*miqureshi@ksu.edu.sa; mohammad.islam@gmail.com*

[**]*amine.achour@laas.fr; a_aminph@yahoo.fr*

[††]*engr_salam@live.com*

Received 16 January 2014
Revised 5 June 2014
Accepted 6 June 2014
Published 1 July 2014

Cadmium sulfide (CdS) and aluminum-doped zinc oxide (Al:ZnO) thin films are used as buffer layer and front window layer, respectively, in thin film solar cells. CdS and Al:ZnO thin films were produced using chemical bath deposition (CBD) and sol–gel technique, respectively. For CBD CdS, the effect of bath composition and temperature, dipping time and annealing temperature on film properties was investigated. The CdS films are found to be polycrystalline with metastable cubic crystal structure, dense, crack-free surface morphology and the crystallite size of either few nanometers or 12–17 nm depending on bath composition. In case of CdS films produced with 1:2 ratio of Cd and S precursors, spectrophotometer studies indicate quantum confinement effect, owing to extremely small crystallite size, with an increase in E_g value from 2.42 eV (for bulk CdS) to $\sim$3.76 eV along with a shift in the absorption edge toward $\sim$330 nm wavelength. The optimum annealing temperature is 400°C beyond which film properties deteriorate through S evaporation and CdO formation. On the other hand, Al:ZnO films prepared via spin coating of precursor sols containing 0.90–1.10 at.% Al show that, with an increase in Al concentration, the average grain size increases from 28 nm to 131 nm with an associated decrease in root-mean-square roughness. The minimum value of electrical resistivity, measured for the films prepared using 0.95 at.% Al in the precursor sol, is $\sim 2.7 \times 10^{-4}\,\Omega \cdot$ cm. The electrical resistivity value rises upon further increase in Al doping level

due to introduction of lattice defects and Al segregation to the grain boundary area, thus limiting electron transport through it.

Keywords: CdS; CBD; Sol–gel; Al:ZnO; resistivity; band gap.

1. Introduction

Cadmium sulfide (CdS) belongs to the family of II–VI semiconductors and has found application in electronic and optoelectronic devices.[1] Due to its intrinsic n-type conductivity, high refractive index ($n \sim 2.5$) and wide bandgap ($E_g \sim 2.42\,\text{eV}$), CdS thin films have been explored for solar photovoltaic (PV) applications.[2] Most chalcogenides based solar modules prefer CdS as buffer layer owing to its favorable conduction-band alignment and compatibility with crystal lattice of the p-type absorber layer.[3] Copper-indium-gallium-sulfide-selenide (CIGSSe) based thin film solar cells that have been reported to exhibit record efficiencies of ~ 20.1 and 16% for research-scale and commercial panels, respectively,[4] use a very thin CdS film as a buffer layer. Since CdS films absorb photons belonging to the blue spectral regime causing a drop in the solar cell efficiency, a low buffer layer thickness is desirable.[5] In thin film form, CdS deposition has been widely studied using chemical as well as vacuum based deposition methods including sputtering,[6] vacuum evaporation,[7] electrodepositon,[8] spray pyrolysis,[9] and chemical bath deposition (CBD).[10] Jaehyeong Lee[11] studied CdS deposition using different techniques and found that CdTe solar cells containing low cost chemical bath deposited (CBD) CdS films show more stable characteristics and increased conversion efficiency.[12] CBD process is preferred for its low cost, low deposition temperature and the possibility to obtain large-area films. CBD process has also been explored for Cd-free buffer layer compositions such as ZnS (Ref. 13) and In_2S_3 (Ref. 14) as an alternative to CdS, albeit with drop in conversion efficiency of the solar cells.

Zinc oxide (ZnO) is a group II–VI semiconductor with direct band gap energy of 3.37 eV. Its electronic conductivity due to the presence of ionized Zn interstitial atoms and electrons, together with the ability to transmit UV/VIS radiation, makes it a promising material for optoelectronic devices. In thin film solar cells, intrinsic and doped ZnO window layer is used as a possible choice to conduct electric currents with low resistive losses among several transparent conductive oxides (TCO). Doping of the ZnO crystal lattice with electron donors such as Al, Ga, In, Ge, Ti, etc.[15] in appropriate concentration improves its electronic properties. Among them, aluminum-doped zinc oxide (Al:ZnO) is the most extensively explored TCO material for window layer application. Sputter deposition of Al:ZnO thin films with electrical resistivity values in the range of 10^{-4} to 10^{-5} Ù.cm is a well-developed processing route that has already entered commercialization phase for CIGS based thin film PV technology. For high quality ZnO films, sol–gel technique offers a simple, low cost and easy-to-control processing route as an alternative to vacuum based techniques. The process involves use of inorganic or organic salts in alcohols and *in situ* alkoxide or alkoxy-complexes formation followed by hydrolysis and polymerization reactions to produce oxide. The electrical resistivity of the sol–gel Al:ZnO films, however, is higher than their sputter deposited counterparts by an order of magnitude. Upon Al doping with 1 at.%, the electrical resistivity of sol–gel spin coated ZnO films was reported to decrease from $6.35 \times 10^2\,\Omega \cdot \text{cm}$ for intrinsic ZnO (Ref. 10) to $4.06 \times 10^{-3}\,\Omega \cdot \text{cm}$.[16] The minimum resistivity value reported for sputtered Al:ZnO films is $5.4 \times 10^{-4}\,\Omega \cdot \text{cm}$.[17]

Although the effect of processing parameters on structure and morphology of CBD CdS films has been previously investigated, we present a systematic parametric study taking into consideration the effect of bath chemistry, deposition time and annealing temperature to find optimum synthesis conditions leading to materials with good electrical and optical properties. Furthermore, sol–gel synthesis of Al:ZnO films with very low electrical resistivity and reasonable level of optical transmittance maybe an important substitute to their sputter deposited counterparts. The present work is part of research efforts to fabricate Cu(In,Ga)Se_2 based thin film solar cells using various solution processing techniques. Due to the important role of such films in solar cell technology, the research findings from two different film compositions are presented in

this paper. Due to their critical importance for band gap alignment of CdS/Cu(In,Ga)Se_2 hetro-junction, CdS films with up to 100 nm thickness were produced via CBD process under different processing conditions. Al:ZnO films with 0.90 to 1.10 at.% Al doping were prepared by spin coating of the precursor solutions. The films were characterized for crystal structure, surface morphology, electrical and optical properties.

2. Experimental

2.1. *Thin film synthesis*

Soda-lime glass (SLG) substrates were initially cleaned in 5 wt.% chromic acid solution for 2 min and then, in 5 wt.% sodium hydroxide solution for 2 min for surface neutralization followed by rinsing in deionized water for removal of any surface residues. For CBD CdS films, the plating bath consisted of hydrated cadmium chloride ($CdCl_2 \cdot 2.5H_2O$), thiourea ($CS(NH_2)_2$) and ammonium hydroxide (NH_4OH). The CdS films were prepared from $CS(NH_2)_2$ decomposition in the presence of $CdCl_2$ in a basic solution with bath pH of ~ 10. Unless explicitly stated, all the films were prepared using Cd^{2+}:$CS(NH_2)_2$ ratio of 1:4 (by mol) with magnetic stirring for homogenous bath composition. The formation of CdS occurs as a result of a series of reaction involving capture of dissolved Cd^{2+} ions to make ammonia complexes and subsequent reaction with S^{2-} coming from $CS(NH_2)_2$. An annealing treatment followed by air cooling was carried out for all the films. The effect of bath temperature (65, 75 and 85°C), deposition time (10–60 min) and annealing temperature (400–500°C) on film surface morphology as well as electrical and optical properties was assessed. The deposited films were dried in a vacuum oven at 130°C for 15 min.

The Al:ZnO films with 0.90, 0.95, 1.05 and 1.10 at.% Al were prepared by spin coating of the sol solution onto substrates at 2000 rpm for 30 s. The precursor sol was made by initially dissolving zinc acetate dehydrate (ZAD) $Zn(CH3COO)_2 \cdot 2H_2O$ into iso-propanol (i-PrOH) and then adding to it monoethanolamine (MEA) ($HO(CH_2)_2NH_2$) drop-by-drop as a stabilizer till the MEA:Zn^{2+} ratio was 0.75. The solution was then magnetically stirred at 60°C for 1 h to ensure complete dissolution of ZAD salt and subsequently aged for 24 h at room temperature. For Al doping with desirable concentration, a 0.2 M solution of aluminum chloride hexahydrate ($AlCl_3 \cdot 6H_2O$) was made in ethanol (EtOH) and certain amount of it was added to ZAD sol such that precursor sol with required Al content (0.90, 0.95, 1.05 or 1.10 at.%) was obtained. The films produced were annealed at 400°C for 1 h.

2.2. *Structural and functional characterization*

For microstructural examination, scanning electron microscope (SEM; JEOL JSM6490A) was operated at voltage, spot size and working distance of 20 kV, 35 nm or 40 nm and 10 mm, respectively. The AFM studies were performed in air through operation in tapping mode to maximize the tip-sample interactions. The probes used were micro-fabricated cantilevers (NSC35; μmasch) with respective values of length, nominal tip radius, spring constant and resonance frequency of 130 mm, < 10 nm, 4.5 N/m and 150 kHz. High-resolution transmission electron microscope (HRTEM) examination was carried out using Hitachi HNAR9000 microscope with accelerating voltage of 300 kV, LaB_6 electron gun and 0.18 nm point-to-point resolution. For TEM measurements, the films were examined by scratching the film and collecting a small fraction of the powder onto copper grid. X-ray diffraction (XRD) studies were performed using X-ray diffractometer (STOE Stadi MP) at 40 kV operating voltage and 40 mA current. For this purpose, Cu-kα radiation was used as a source of incident monochromatic X-ray beam, while the values of step size and dwell time were maintained at 0.04° and of 3 s per step, respectively. The average crystallite size was determined using Scherrer equation, $t = 0.94\lambda/(\beta_{1/2} \cos\theta)$, where λ is 0.154 nm and $\beta_{1/2}$ is full width at half maximum (in radians) obtained from XRD pattern and 0.94 is the value of dimensionless shape factor for spherical crystallites.

Functional properties such as optical transmittance and band gap values were determined using Spectrophotometer (Labomed UV 2500), The optical band gap value (E_g) of the films can be computed through extrapolation of the $(\alpha h\nu)^2$ versus $h\nu$ curve, since photon energy is E_g when $(\alpha h\nu)^2$ becomes zero. For that purpose, the value of optical absorption coefficient (α) is calculated using film thickness and optical transmittance at a certain wavelength. The

electrical resistivity, carrier concentration and carrier mobility values were measured using Van der Pauw variable temperature Hall Effect measurement system (Ecopia HMS-5000). More details about the system and measurement procedure can be found elsewhere.[17]

3. Results and Discussion

3.1. *CBD CdS films*

Both bath temperature and substrate immersion time influence CdS film characteristics such as thickness and surface morphology. The effect of temperature and time on film microstructure was investigated for 75°C and 85°C bath temperature and substrate immersion time of 20 min and 40 min, as shown in Figs. 1(a)–1(d). The light regions of SEM images represent CdS deposit whereas dark isolated areas indicate underlying glass substrate. Comparison of deposit features upon film synthesis at 75°C and 85°C reveals an increase in nuclei surface density upon raising the bath temperature. For bath temperature of 65°C, few isolated CdS nuclei formed over glass substrate (not shown). Little or no film deposition at ≤ 65°C is presumably due to high bath stability and extremely slow reaction kinetics. As shown in Fig. 1(b), film growth at 85°C produces in a dense, continuous deposit with fewer voids. High magnification view of surface microstructures, presented in Figs. 1(c) and 1(d), indicates the effect of substrate immersion time at 85°C bath temperature. Since film deposition occurs through controlled nucleation of CdS particles over the substrate, if sufficient time is allowed, the nuclei formed at the surface will experience growth and coalesce due to diffusion-limited Ostwald ripening, resulting in a continuous film by following "island growth" model. Therefore, an increase in bath temperature or dipping time or both leads to more homogeneous coverage of the substrate beside an increase in film thickness. The film thickness

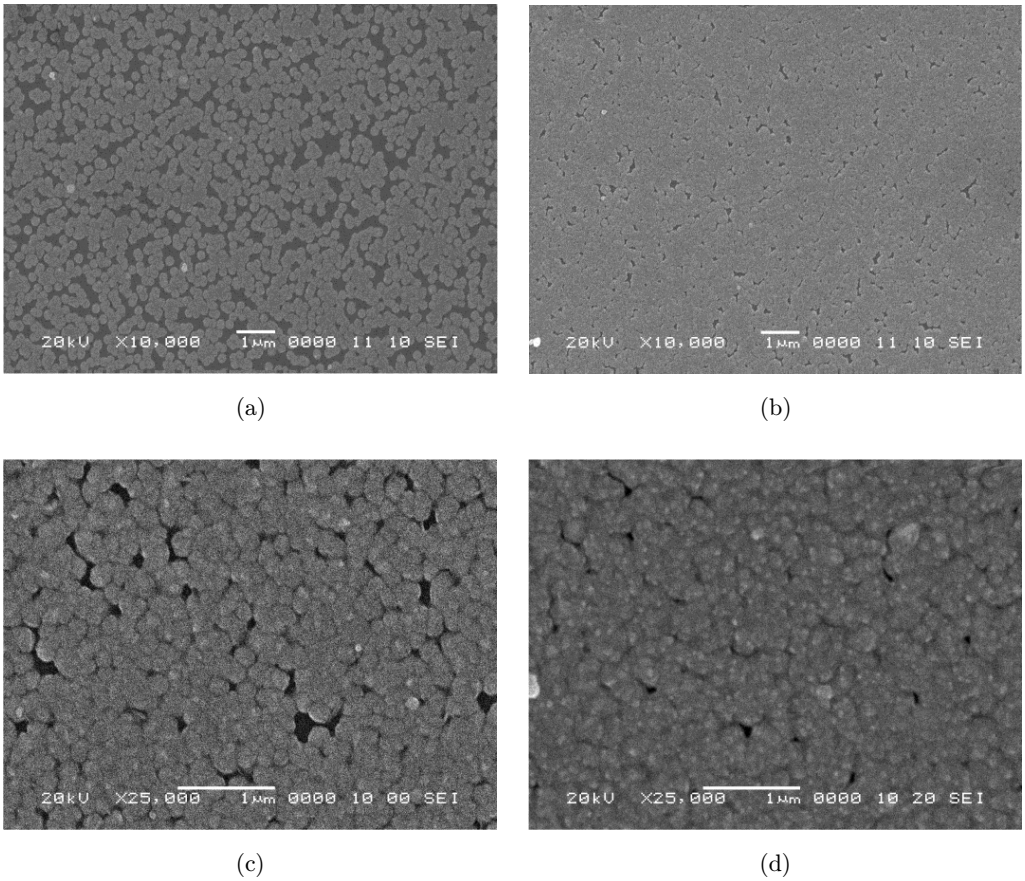

Fig. 1. SEM of the CdS film surfaces comparing the effect of (a), (b) bath temperature (75°C and 85°C for 30 min immersion) and (c), (d) dipping time (20 min and 40 min at 85°C).

values were estimated using interferometer and were found to be up to 100 nm for all the samples.

The composition and crystal structure of the films was investigated through XRD studies. The XRD patterns produced at 75°C (30 min) and 85°C (20, 40 and 60 min) are shown in Fig. 2. Absence of any peaks characteristic of CdS phase confirms very little or no film deposition resulting in partial coverage of the substrate surface at 65°C. For bath temperature of 85°C, an increase in CdS film growth rate due to heterogeneous reaction at the immersed glass substrate, was observed as manifested by appearance and gradual increase in peak intensities characteristic of different crystallographic planes belonging to the CdS lattice. With relative intensity in descending order, the peaks are present at 2θ values of 26.5°, 44.0° and 52.3°, and can be indexed as (111), (220) and (311) planes of the cubic structure (JCPDS-80–0019), respectively. Since CdS films can possess both stable hexagonal and metastable cubic structures with peak positions for (111) and (220) planes of the cubic (zincblende) structure being identical to those of (002) and (110) planes of the hexagonal (wurtzite) CdS lattice structure, the XRD patterns yield inconclusive evidence regarding the films that are hexagonal or cubic or a mixture of both structures. For the same bath chemistry and temperature, an increase in deposition time only appears to affect the degree of film crystallinity as evident from relative intensities of the diffraction peaks. On the other hand, for CdS film produced using 1:2 molar ratio of Cd and S precursors, a significant shift in the position of peaks toward greater 2θ values is noticed along with much larger extent of peak broadening. While the former trend is characteristic of a decrease in interplanar spacing with subsequent increase in the band gap energy, the latter trend implies high transmittance over a broad range of optical spectral regime beside appearance of absorption edge. Peak broadening indicates that CdS films are nanocrystalline in nature and the FWHM shows the crystallite size to be in the range of $\sim$12 nm to 16 nm, except for sample 8 for which the crystallite size is found to be few nanometers. For colloidal CdS nanocrystals, the growth

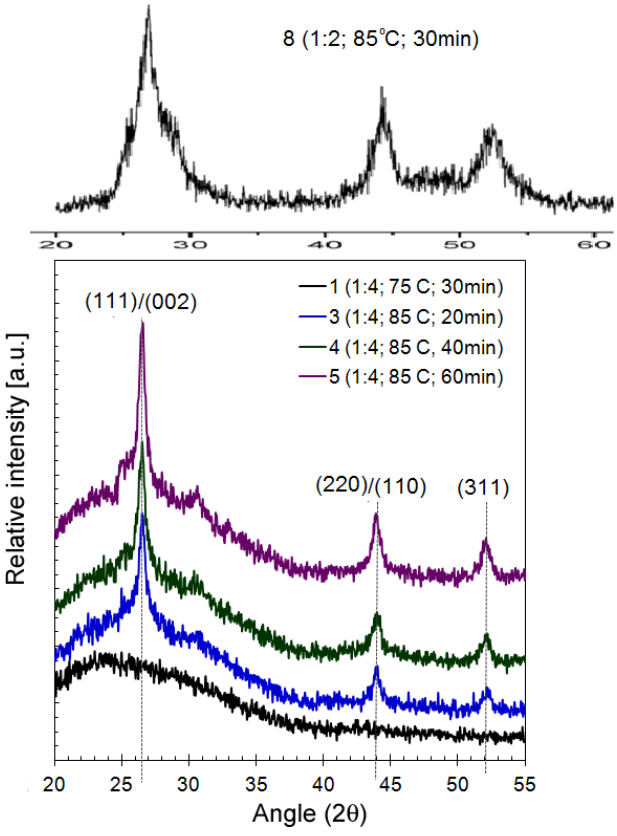

Fig. 2. XRD patterns of CdS films produced under different processing conditions (Table 1).

is explained by a combined model containing both diffusion-limited Ostwald ripening of CdS particles on glass substrate following the Lifshitz–Slyozov–Wagner (LSW) theory and the reaction at the surface. Kostoglou *et al.*[18] modeled the CdS thin film growth by CBD method by taking into account the nucleation, particle coagulation, particle growth by ionic addition and particle deposition. They found that CdS nuclei continuously develop with time over the substrate and grow which contradicts the layer by layer or crystallization theory.

HRTEM examination of the film (sample 4) confirms polycrystalline nature of the deposits with crystallite size of the order of few nanometers, as shown in Fig. 3. The selected-area electron diffraction (SAED) pattern (inset in Fig. 3) indicates presence of diffraction rings characteristic of (hkl) planar indices of the cubic (zincblende) CdS structure (JCPDS 89-0440). Thus, HR-TEM studies resolve the ambiguity concerned with crystal structure of the CdS films. While annealing at 400°C significantly enhances electrical characteristics of CdS films through densification and crystallization, similar treatment at or above 450°C under atmospheric conditions results in loss of crystallinity due to sulfur evaporation and cadmium oxide (CdO) formation. The presence of CdO in the films annealed at such temperatures can be attributed to adsorbed water that may act as oxidizing agent at temperatures beyond 400°C. Another factor responsible for CdO formation is the presence of $Cd(OH)_2$ precipitates in films that decompose during annealing to produce CdO and water vapors. The latter acts as a byproduct and further enhances the extent of CdO formation.

Keeping other processing parameters the same (85°C, 40 min; annealing at 400°C, 30 min), an increase in the cadmium chloride to thiourea ratio to 1:2 causes a strikingly different CdS film surface morphology consisting of well-defined round, granular structure with an average size of the order of few nanometers. High magnification SEM image and the 3-dimensional surface topography, presented in Fig. 4, indicate very smooth film surface along with presence

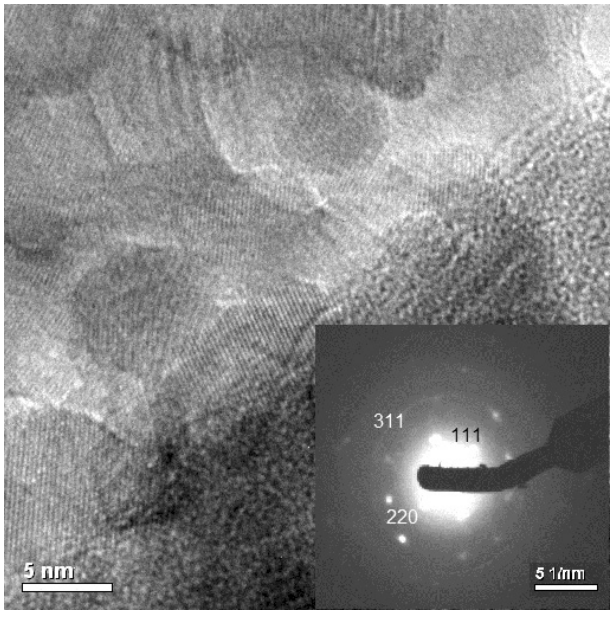

Fig. 3. (a) HR-TEM microstructure and (b) SAED pattern of the CdS film (85°C, 40 min).

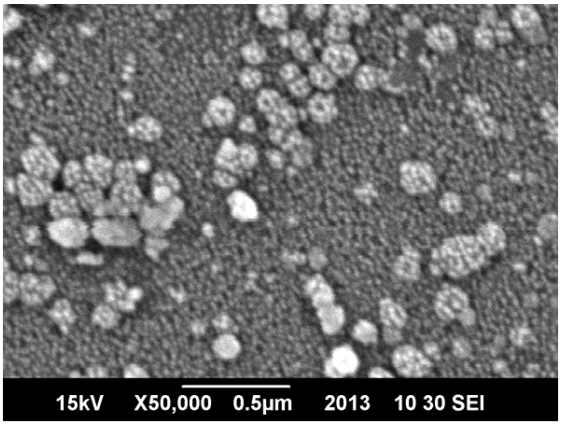

(a)

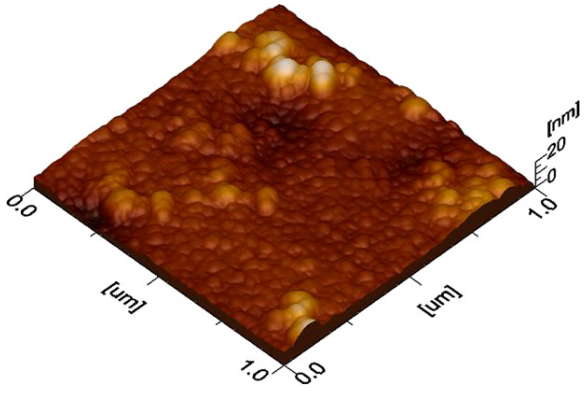

(b)

Fig. 4. CBD CdS film produced with Cd^{2+}:$CS(NH_2)_2$ molar ratio of 1:2 (85°C, 30 min): (a) High magnification SEM microstructure and (b) the three-dimensional morphology from AFM scan.

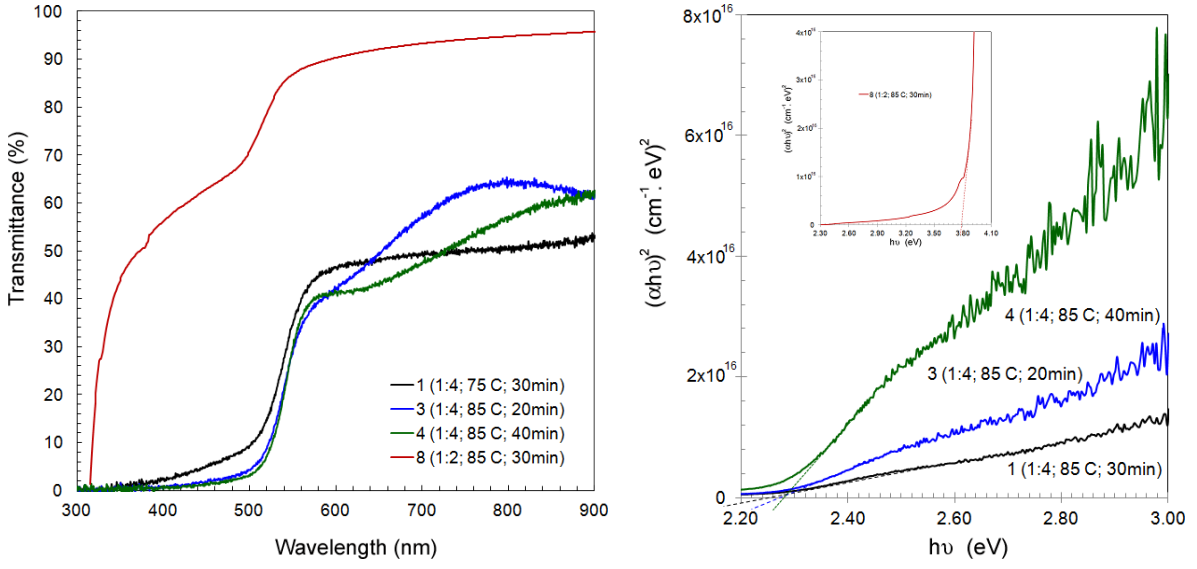

(a) (b)

Fig. 5. (a) Transmittance spectra and (b) $(\alpha h\nu)^2$–$h\nu$ plot of the transmittance data for extrapolation of E_g values for CBD CdS films.

of small clusters. For a $2 \times 2\,\mu$m scan area, the average surface roughness is estimated to be ~ 2.63 nm.

The transmission spectra and $(\alpha h\nu)^2$–$(h\nu)$ graphs of the CdS films deposited using $CdCl_2$:$CS(NH_2)_2$ of 1:4 (mol) (samples 1, 3, 4) and 1:2 (sample 8) are presented in Fig. 5. The CdS films produced with 1:4 molar ratio of Cd and S precursors exhibit low transmittance values with an increase in maximum value from $\sim$51% to 65% upon increasing the bath temperature from 75°C to 85°C. For film growth at 85°C, the deposition time does not seem to produce significantly different films as indicated by similar values of maximum percent transmittance and the presence of an absorption edge at higher wavelengths, presumably due to less light scattering from the smooth film surface. This absorption edge, positioned at $\sim$600 nm wavelength, is the primary cause of a sub-band gap and is indicative of defects formation in the films. In case of CdS film synthesis using $CdCl_2$:$CS(NH_2)_2$ of 1:2, high percent transmittance value of 90% or above was noticed with a shift in absorption edge to $\sim$380 nm wavelength which implies a reduction in the bandgap value. The band gap energy computed from $(\alpha h\nu)^2$–$(h\nu)$ plots (Fig. 5(b)) and the corresponding wavelength values for different CdS films are listed in Table 1. For sample 8, the E_g value has

Table 1. Processing conditions, physical and optical properties of the CBD CdS films.

ID	Synthesis conditions	Thickness (nm)	Crystallite size (nm)	Transmittance (%)	Wavelength (nm)	Band gap (eV)
1	75°C, 30 min	91	—	49.7	551.4	2.25
2	85°C, 30 min	89	14.5	67.4	544.2	2.28
3	85°C, 20 min	60	17.1	65.3	539.4	2.30
4	85°C, 40 min	79	10.5	62.3	546.6	2.27
5	85°C, 60 min	95	15.1	56.5	—	—
6	*450°C, 30 min	—	15.5	75.6	—	—
7	*500°C, 30 min	—	—	33.2	—	—
8	1:2, 85°C, 30 min	55	$\sim$1.5	96.9	347.5	3.57
					330.0	3.76

* Films deposited under same conditions as those for sample 4 but annealed at different conditions.

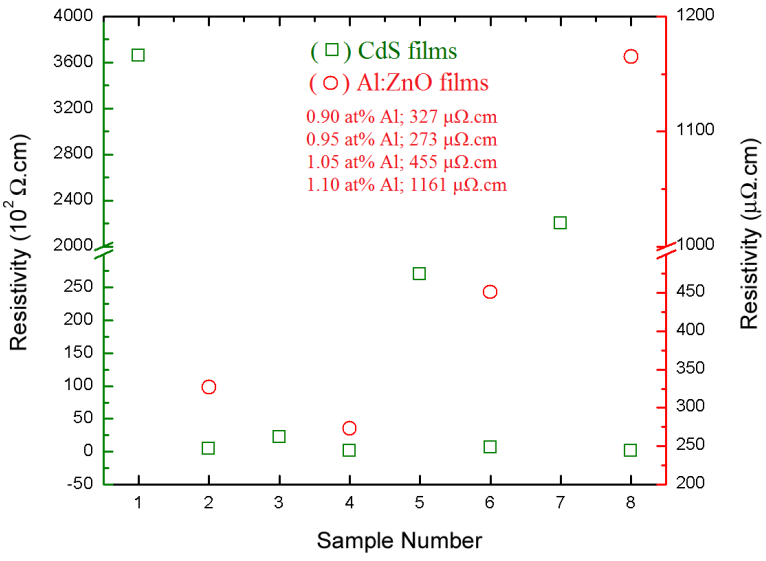

Fig. 6. Electrical resistivity values for CdS and Al:ZnO films determined from Van der Pauw method.

significantly increased due to quantum confinement effect, in accordance with earlier reports.[19,20] Upon annealing at 500°C (sample 7), the value of %T is found to be drastically reduced (not shown) due to CdO formation with an associated drop in the E_g value caused by larger grain size, re-organization of the film, and changes in film composition due to sulfur evaporation and CdO formation.

The electrical resistivity of the CdS films was measured in darkness by means of Hall Effect apparatus using indium-tin contacts. The films show n-type conductivity with carrier concentration of the order of 10^{11}–$10^{14}\,\mathrm{cm}^{-3}$. Films produced at 85°C exhibit smooth, conformal growth with improved crystalline quality, denser morphology, large grain size and less grain boundary area, all of which cause reduction in electrical resistivity. With an increase in thickness and better crystal quality, the values of electrical resistivity and the carrier concentration initially decrease while those of carrier mobility increase. This increase in mobility value can be explained by the fact that charge carriers generated by photo-excitation get trapped at grain boundaries, thus resulting in a lower inter-grain barrier height allowing these carriers to move around with relatively less resistance.[20] The increase in electrical resistivity manifested by the films produced with longer deposition time (> 40 min) maybe attributed to film cracking, higher dislocation density and crystallographic imperfections in the films. On the other hand, electrical resistivity of the films also significantly drops upon annealing at temperatures beyond 400°C due to partial degradation of CdS through conversion into CdO phase. The electrical resistivity data for different CdS films is shown graphically in Fig. 6.

3.2. *Sol–gel Al:ZnO films*

AFM studies of Al-doped ZnO films (Al:ZnO) with Al doping level of 0.90, 1.05 and 1.10 at.% Al was carried out, as shown in Fig. 7. All the films exhibit dense structure with little or no porosity in the film surface. For Al:ZnO films with Al concentration of 0.90, 1.05 and 1.10 at.%, the average grain size is estimated to be 28, 46 and 131 nm, respectively, indicating a gradual increase with increasing Al concentration. The 3-dimensional morphology revealed slight drop in the value of root mean square (RMS) roughness from 8.6 nm to 4.8 nm upon increasing Al concentration. Figures 7(a) and 7(b) represent surface topography of the Al:ZnO film (0.90 at.% Al) with scan size of $6 \times 6\,\mu$m and 500×500 nm to illustrate surface features at two different length scales. The incorporation of Al into ZnO during film growth is confirmed from energy dispersive spectrum (EDS) given in Fig. 7(e). Among the four samples, Al:ZnO film prepared from 0.95 at.% Al reveals minimum Al and maximum O content in the deposited film, as pointed out by the EDS analysis (not shown). In contrast, the Al content is maximum in the film

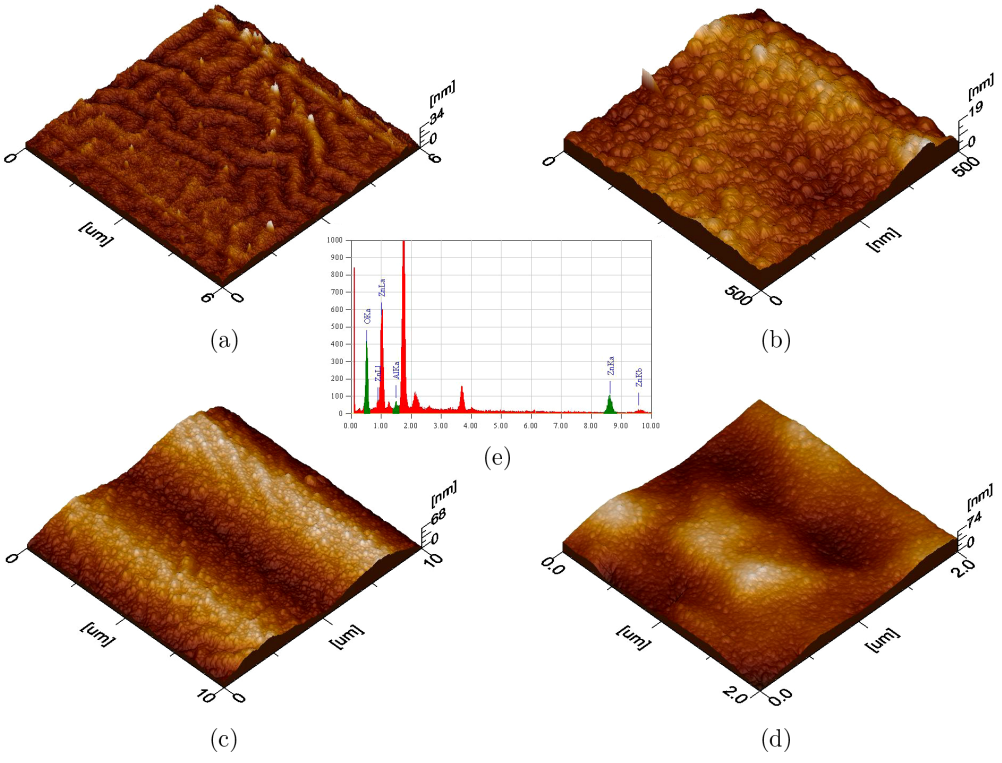

Fig. 7. (a)–(d) AFM images of spin coated Al:ZnO films using precursor sols containing different Al concentrations: (a), (b) 0.90 at.%, (c) 1.05 at.% and (d) 1.10 at.%; (e) EDS spectrum of Al:ZnO film.

prepared from solution containing 1.10 at.% Al in the precursor sol. Since the error margin is large during EDS studies, due to very small amounts of Al in the films, the EDS data only provide qualitative results.

The values of electrical resistivity for Al:ZnO films are plotted in Fig. 6 (series with red marker). For the films produced with increasing Al concentration in the precursor sol, the electrical resistivity slightly decreased showing a minimum value of $2.73 \times 10^{-4}\,\Omega \cdot \text{cm}$ followed by gradual increase to a maximum value of $\sim 1.16 \times 10^{-3}\,\Omega \cdot \text{cm}$. As Al concentration is increased, Al^{3+} captures more oxygen in competition with Zn^{2+} because of its larger nuclear charge causing a reduction in crystalline quality of the films. Another possible explanation maybe that relatively smaller ionic radius of Al (0.56 Å) than that of Zn (0.74 Å) leads to occupation of interstitial positions by Al, causing distortion of the ZnO lattice structure. Among the range of precursor sol compositions investigated, Al:ZnO film prepared with 0.95 at.% Al show minimum electrical resistivity value.

4. Conclusion

CdS films prepared using CBD process are sub-100 nm thick with cubic structure, dense, crack-free surface morphology and crystallite size from few nanometers to ~ 17 nm, depending on Cd^{2+}: $CS(NH_2)_2$ ratio in the precursor solution. Upon increasing the Cd^{2+}: CS $(NH_2)_2$ molar ratio from 1:4 to 1:2, optical transmittance rises to a maximum value of $> 95\%$ with enhancement in E_g value from 2.42 eV (for bulk CdS) to 3.76 eV, thus pointing toward quantum confinement effect. There is also an associated shift in absorption edge to low wavelength (~ 330 nm) with sub-band gap energy value of ~ 3.56 eV. The electrical resistivity of the films after annealing at 400°C for 30 min is found to be $\sim 10^2\,\Omega \cdot \text{cm}$ and increases upon annealing at higher temperatures due to film deterioration through S evaporation and CdO formation. In case of sol–gel spin coated Al:ZnO films, the average grain size increases from 28 nm to 131 nm with an associated decrease in RMS roughness upon increasing Al concentration from 0.90 to 1.10 at.%. The value

of electrical resistivity depends on the extent of Al incorporation with the minimum value of $2.7 \times 10^{-4}\,\Omega \cdot \mathrm{cm}$ for films prepared using 0.95 at.% Al in the precursor sol. Upon further increase in Al doping level, the electrical resistivity value increases probably due to introduction of lattice defects and Al segregation to the grain boundary area thus limiting electron transport through it.

Acknowledgements

The authors would like to extend their sincere appreciation to the Deanship of Scientific Research at King Saud University for its funding of this research through the Research Group Project No. RGP-VPP-283.

References

1. L. Wenyi, C. Xun, C. Qiulong and Z. Zhibin, *Mater. Lett.* **59** (2005) 1.
2. E. Çetinörgü, C. Gümüş and R. Esen, *Thin Solid Films* **515** (2006) 1688.
3. B. T. Ahn, L. Larina, K. H. Kim and S. J. Ahn, *Pure Appl. Chem.* **80** (2008) 2091.
4. H. Katagiri, K. Jimbo, S. Yamada, T. Kamimura, W. S. Maw, T. Fukano, T. Ito and T. Motohiro, *Appl. Phys. Exp.* **1** (2008) 041201.
5. H. R. Moutinho, D. Albin, Y. Yan, R. G. Dhere, X. Li, C. Perkins, C. S. Jiang, B. To and M. M. Al-Jassim, *Thin Solid Films* **436** (2003) 175.
6. E. M. Feldmeier, A. Fuchs, J. Schaffner, H. J. Schimper, A. Klein and W. Jaegermann, *Thin Solid Films* **519** (2011) 7596.
7. M. Tomakin, M. Altunbaş, E. Bacaksiz and Ş. Çelik, *Thin Solid Films* **520** (2012) 2532.
8. K. Zarębska and M. Skompska, *Electrochim. Acta* **56** (2011) 5731.
9. S. Aksay, M. Polat, T. Özer, S. Köse and G. Gürbüz, *Appl. Surf. Sci.* **257** (2011) 10072.
10. S. Salam, M. Islam, M. Alam, A. Akram, M. Ikram, A. Mahmood, M. Khan and M. Mujahid, *Adv. Nat. Sci. Nanosci. Nanotechnology* **2** (2011) 045001.
11. J. Lee, *Appl. Surf. Sci.* **252** (2005) 1398.
12. X. Mathew, J. S. Cruz, D. R. Coronado, A. R. Millán, G. C. Segura, E. R. Morales, O. S. Martínez, C. C. Garcia and E. P. Landa, *Solar Energy* **86** (2012) 1023.
13. G. L. Agawane, S. W. Shin, M. S. Kim, M. P. Suryawanshi, K. V. Gurav, A. V. Moholkar, J. Y. Lee, J. H. Yun, P. S. Patil and J. H. Kim, *Current Appl. Phys.* **13** (2013) 850.
14. B. Asenjo, C. Guillén, A. M. Chaparro, E. Saucedo, V. Bermudez, D. Lincot, J. Herrero and M. T. Gutiérrez, *J. Phys. Chem. Solids* **71** (2010) 1629.
15. H. T. Cao, Z. L. Pei, J. Gong, C. Sun, R. F. Huang and L. S. Wen, *Surf. Coat. Technol.* **184** (2004) 84.
16. S. Salam, M. Islam and A. Akram, *Thin Solid Films* **529** (2012) 242.
17. Z. B. Ayadi, L El Mir, K Djessas and S Alaya, *Nanotechnology* **18** (2007) 445702.
18. M. Kostoglou, N. Andritsos and A. J. Karabelas, *Thin Solid Films* **387** (2001) 115.
19. R. Das and S. Pandey, *Int. J. Mater. Sci.* **1** (2011) 35.
20. U. Manzoor, M. Islam, L. Tabassam and S. Rahman, *Physica E* **41** (2009) 1669.